International Journal of Minerals, Metallurgy and Materials
Accepted manuscript, https://doi.org/10.1007/s12613-019-1954-y

Liquation Cracking in the Heat-Affected Zone of IN939 Superalloy Tungsten Inert Gas Weldments

H. Kazempour-Liasi[1,2], *M. Tajally*[1], *and H. Abdollah-Pour*[1]

1) Faculty of Materials and Metallurgical Engineering, Semnan University, Semnan, Iran

2) Metallurgy Department, Niroo Research Institute, Tehran 14686, Iran

Corresponding author: m_tajally@semnan.ac.ir (M. Tajally), Telfax: +98-23 33654089

Abstract

The main aim of this study was to investigate liquation cracking in the heat-affected zone (HAZ) of the IN939 superalloy upon tungsten inert gas welding. A solid solution and age-hardenable filler metals were further studied. On the pre-weld heat-treated samples, upon solving the secondary γ′ particles in the matrix, primary γ′ particles grew in the base metal to "ogdoadically diced cubes" of about 2 μm in side length. The pre-weld heat treatment reduced the hardness of the base metal to about 310 HV. Microstructural studies using optical and field-emission scanning electron microscopy revealed that the IN939 alloy was susceptible to liquation cracking in the HAZ. The constitutional melting of the secondary, eutectic, and Zr-rich phases promoted the liquation cracking in the HAZ. The microstructure of the weld fusion zones showed the presence of fine spheroidal γ′ particles with a size of about 0.2 μm. The phases increased the hardness of the weld pools after the post-weld heat treatment to about 350 and 380 HV for the Hastelloy X and IN718 filler metals, respectively. Application of a suitable solid solution filler metal could partially reduce the liquation cracking in the HAZ of IN939 alloy.

Keywords: IN939; superalloy; TIG; weld; HAZ; liquation; cracking.

INCONEL (IN) and Hastelloy alloys are trade names of the Special Metals Corporation group of companies

1. Introduction

Precipitation-strengthened Ni-based superalloys are widely used in the manufacture of hot gas path components for aircraft and industrial gas turbines that are designed for high-stress and high-temperature operating conditions. The fusion welding process has been frequently used for joining and repairing these components [1]. The tungsten inert gas (TIG) process provides a conventional approach to repair the welding of Ni-based superalloy-made components [2-5]. The weldability of Ti and Al-rich superalloys is poor because of their high susceptibility to cracking in the heat-affected zone (HAZ) due to the formation of the γ′ precipitate [1]. As a Ni-based superalloy, IN939 can be hardened by precipitation of the γ′ phase and it is designed for use in the blades of gas turbines [6, 7]. During the welding process, the base metal adjacent the fusion zone is susceptible to high temperatures between the liquidus and effective solidus temperature, which may lead to local melting in the HAZ. Liquation cracking can then occur as the liquid cannot withstand the strain during the welding process. The tendency to liquation cracking is increased with TIG due to the high heat input [8].

Liquation cracking occurs in the HAZ due to melting of the products that are terminally solidified at the interdendritic region. Examples of such products include MC carbides, γ-γ′ colonies, borides (M_3B_2 and M_5B_3), sulfocarbides (M_2SC), and intermetallic compounds (Ni_7Zr_2 and γ′-Ni_3(Al, Ti)) [2-5, 9, 10].

The use of electron beam welding can, to a certain extent, reduce liquation cracking, but cannot eliminate it completely [10-13]. The chemical composition and initial microstructure can also affect the liquation cracking [10, 14, 15]. Welding under as-cast and over-aged conditions intensifies liquation cracking due to the higher volumetric fraction of the carbides and γ′ particles and coarsening of the γ′ particles, respectively [14, 15].

Most studies on the liquation cracking have focused on the IN738 alloy [2, 9, 12-15]. With respect to liquation cracking of the IN939 superalloy, existing literature has merely reported the effects of the γ′ morphology on the cracking [16,17]. The objective of this study is to reduce the HAZ cracking in IN939 TIG weldments. In this study, we consider the effects of pre-weld heat treatment, filler metals, and post-weld heat treatment (PWHT) on the liquation cracking of IN939. Additionally, the Hastelloy X (solid solution) and IN718 (age-hardenable) filler metals are used. Furthermore, various pre- and PWHT are applied and their effects on HAZ cracking are investigated.

2. Materials and methods

Coupons with dimensions of 2 × 2 × 8 cm were cut from IN939 gas turbine blades using a wire electrical discharge machine (WEDM). The chemical composition of the base metal alloy (IN939) and filler metals (Hastelloy X and IN718) are presented in Table 1. A sample coupon is shown in Fig. 1.

Table 1. Chemical composition of the studied filler metals and base metal alloy (wt. %) [2, 3].

Alloy	Al	Ti	B	W	Ta	Cr	C	Fe	Nb	Si	Mn	Zr	Co	Ni
IN939	2.0	3.7	0.014	2.2	1.4	22.5	0.15	0.5	1.1	0.2	0.2	0.14	19	Bal.
Hastelloy X	2	-	-	0.6	-	22	0.15	18	-	-	-	-	1.5	Bal.
IN718	0.5	0.9	-	-	-	19	0.08	18.5	5.1	-	-	-	-	Bal.

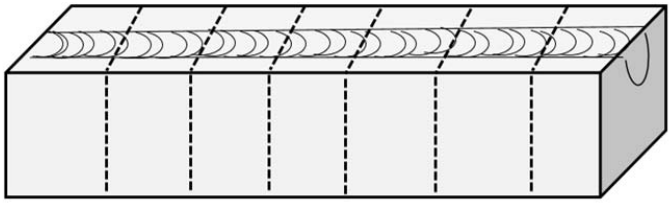

Figure 1. The prepared and welded coupons under the bead weld configuration in this work.

The present research was conducted in two steps. First, the sample coupons were subjected to a pre-weld heat treatment to investigate the liquation cracking. In the next step, the formation of strain-age cracks around the weld zone after the PWHT was investigated. The pre- and post-weld heat treatments are described in Table 2.

A solid solution (Hastelloy X) and precipitation-hardenable alloy (IN718) were used as filler metals. TIG welding with a 10-V DC current at 60 A was applied with a 1.2-mm diameter wire of the filler metal.

The welded coupons were sectioned transversely to the welding direction using the WEDM. The cut surface of each coupon was then polished, etched, and examined for susceptibility to cracking by measuring the total crack length (TCL) per section. The specimens were etched in a solution containing 0.3 g of MoO_3, 10 ml of HNO_3, 10 ml of HCL, and 15 ml of H_2O. Optical microscopy (OM) was used for the TCL measurements. Prior to the microstructural study, the

samples were ground to 0.5 mm to remove the oxidized and/or depleted layers. The microstructural characteristics were analyzed using OM and field-emission scanning electron microscopy (FESEM) on a TESCAN-MIRA3. The chemical composition of the secondary phases studied using energy-dispersive X-ray spectroscopy (EDS). The Vickers hardness method was used with a load of 30 kg and loading time of 10 s to investigate the relationship between the hardness of the filler metal and the amount of cracking around the weld. Elemental distribution calculations and thermodynamics analysis were performed in the JMatPro Software Package in conjunction with the Ni-DATA database.

Table 2. Pre- and post-weld heat treatment cycles adopted in this work.

Heat treatments	Description
Pre-weld heat treatment	1160°C /4h/FC/ to 920°C(rate 0.5°C/min)/AC
Post-weld heat treatment	1160°C/4h/AC+1000°C/6h/FAC+900°C/24h/AC+700°C/16h/AC

FAC: fast air cool, AC: air cool, FC: furnace cool

3. Results and discussion

3.1. Microstructural examination and microcracks in the HAZ

The optical micrographs captured across the HAZ on the samples welded with the studied filler metals are shown in Fig. 2. The samples welded with either IN718 or Hastelloy X exhibited cracks in the HAZ. In terms of microstructure, the as-received IN939 was made up of a primary (MC) and secondary ($M_{23}C_6$) carbides, and primary and secondary γ′ particles with a fine particle size of 20 to 150 nm (Fig. 3). In this case, the hardness of the base alloy was about 470 HV. The samples were subjected to a pre-weld heat treatment to reduce the hardness and increase the weldability of the specimens [18, 19], upon which the base metal had its hardness reduced to about 310 HV and its microstructure was comprised of γ/ γ′ eutectic (Fig. 4-a,b), η plate phases in a γ matrix (Fig. 4-c) and primary MC carbides (Fig. 4-d), very coarse primary γ′ particles (~1 to 2 μm). Liquation cracking was expected due to the presence of eutectic microstructures and coarse γ′ particles. Moreover, the presence of η phases in the microstructure

(Fig. 4-c) could contribute to crack formation in the HAZ via a constitutional liquation mechanism [20].

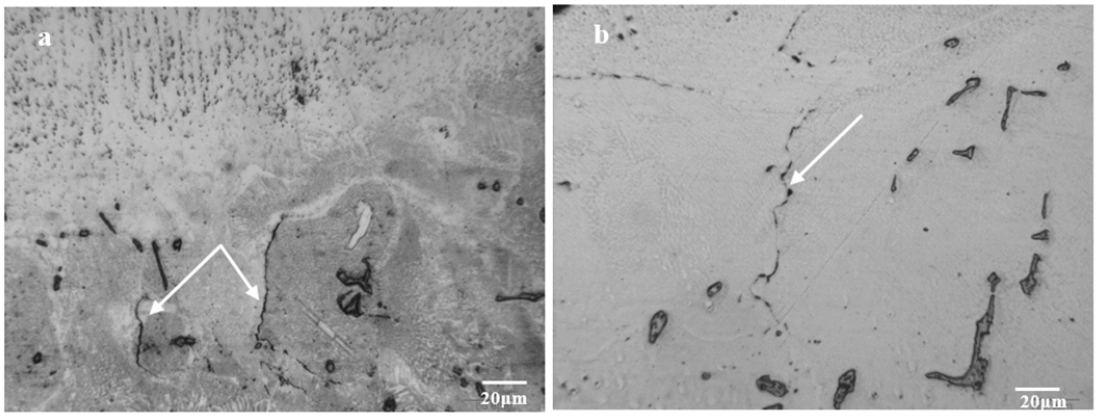

Figure 2. Optical micrographs of cracking in the heat-affected zone (HAZ) on the samples welded with (a) Hastelloy X and (b) IN718 as filler metal. Cracks are marked by arrows.

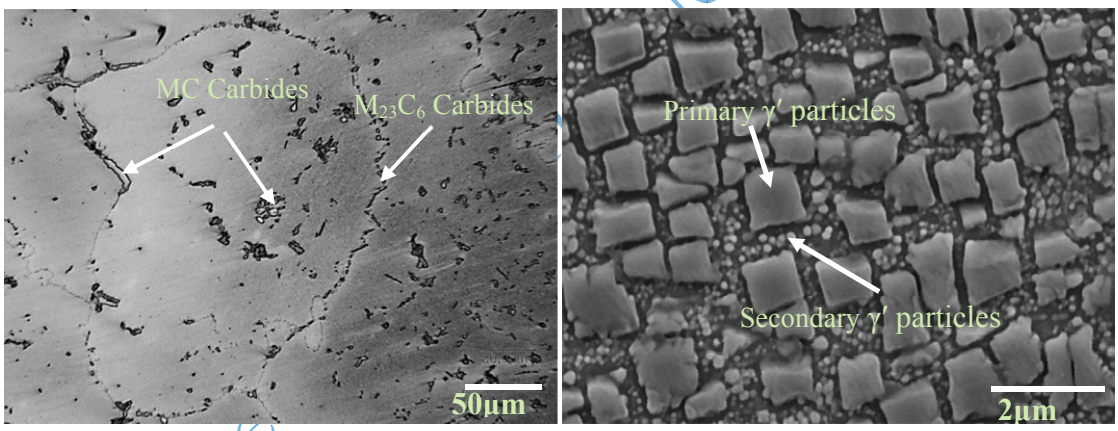

Figure 3. (a) Optical micrograph and (b) Field-emission scanning electron microscopy (FESEM) image of the microstructure of as-received IN939. The primary (MC) and secondary ($M_{23}C_6$) carbides, and primary and secondary γ′ particles are observed in the base metal.

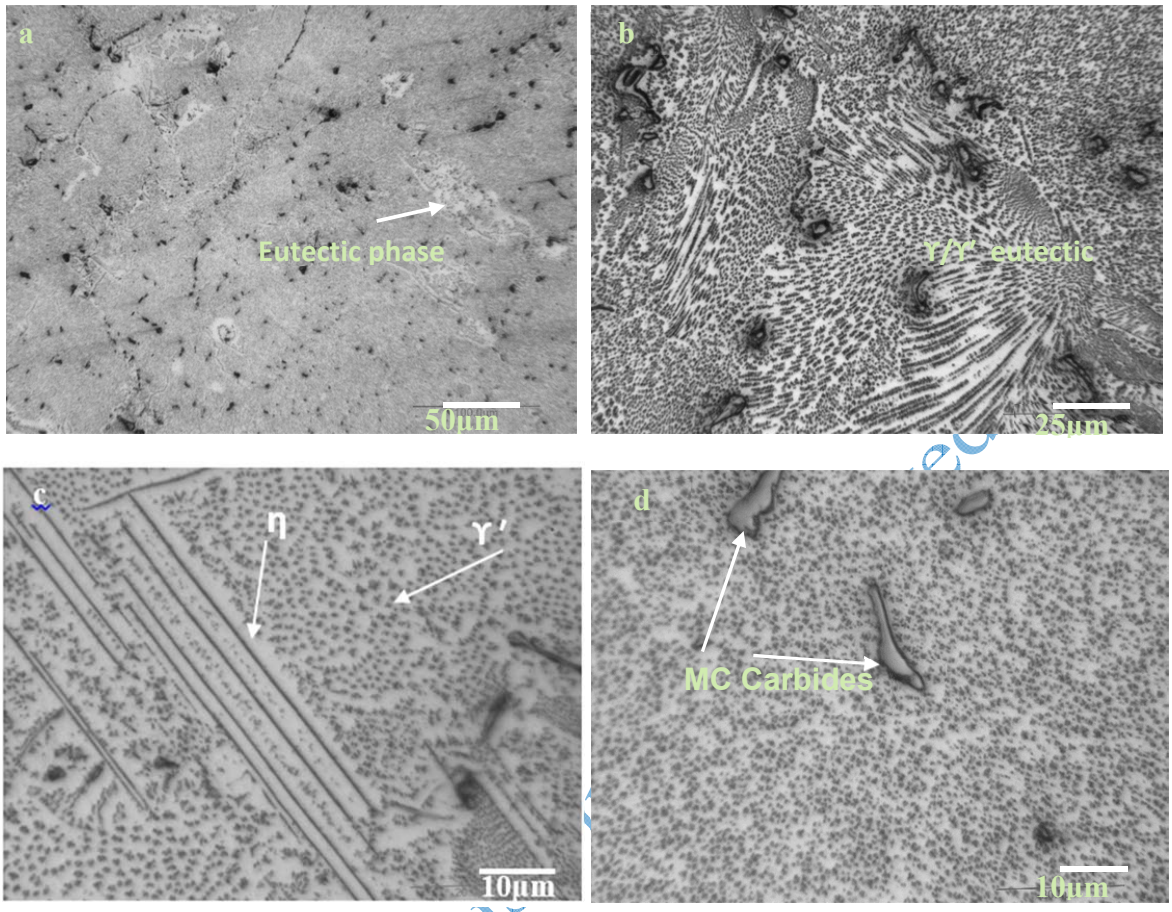

Figure 4. Optical micrographs of the pre-weld heat-treated samples. The γ′ particles and eutectic and η phases are observed in the base metal.

Fig. 5 shows FESEM images of the γ′ particles in the pre-weld heat-treated samples. According to Fig. 5-c, this condition led to the growth of primary γ′ particles into cubic and "ogdoadically diced cubic" particles 12 µm in size, and complete dissolution of the secondary γ′ particles in the matrix with no chance of nucleation or growth (Fig. 5-c). This type of γ′ particle forms during the coarsening of coherent γ′ particles. The driving force for this type of growth is provided by minimization of the misfit energy and the interface energy between γ and γ′ phases. In this case, the cubic primary γ′ particles grow from the corners [21, 22].

Although the primary γ′ particles were quite clearly molten adjacent to the weld pool (Fig. 5-a), the cores of the γ′ particles exhibited limited melting, while melting was more evident in areas farther from the weld pool (Fig. 5-b). The partial melting of the γ′ particles away from the weld

pool was due to insufficient temperature and time for the process to occur. These microstructural changes are caused by temperature gradients toward the weld pool during the welding process [8, 20].

Fig. 6 shows the FESEM image of primary carbide and γ′ particles in the HAZ. The primary carbide and γ′ particles underwent melting during the welding process, clearly indicated by the melting around the particles.

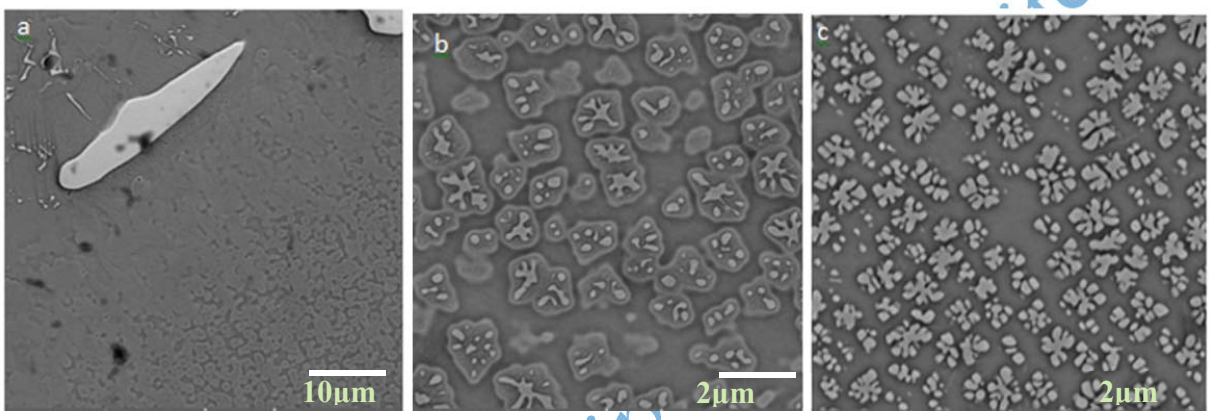

Figure 5. FESEM images of the γ′ particles in the specimen welded with Hastelloy X as filler metal at (a) the interface between the weld pool and the base metal, (b) a distance of about 200 μm from the weld line, and (c) the base metal. The "ogdoadically diced cubic" γ′ particles are observed in the microstructure.

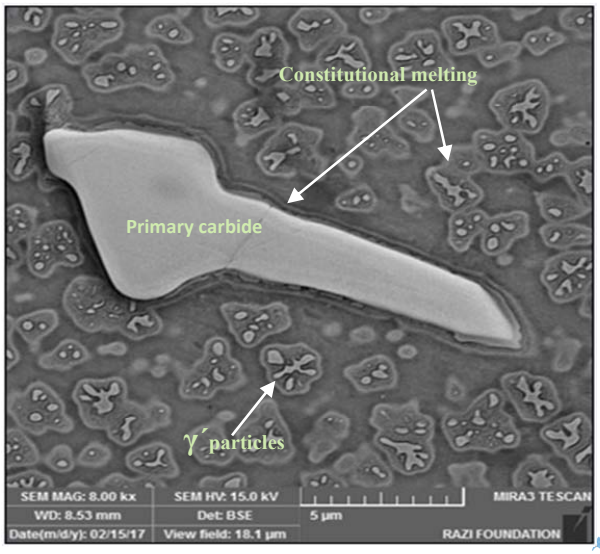

Figure 6. FESEM images of the constitutional melting of the carbide and γ´ particles around the weld pool on the specimen welded with Hastelloy X as filler metal.

Fig. 7 shows an example of cracking in the HAZ of the specimens welded with Hastelloy X and IN718 as filler metal. The intergranular cracking that occurred upon the formation and growth of cracks around the particles of the secondary phases, *e.g.,* primary carbide and γ′ particles (Figs. 7-a, b), was associated with the constitutional liquation mechanism (Figs. 7-c, d).

Development of the melting zone around the weld pool and diffusion of the liquid phase into the grain boundaries or phase-matrix interface would cause liquation cracking in the HAZ [5, 6]. Specifically, the intergranular liquation and resultant cracks are due to the non-equilibrium liquation of the secondary phases in the pre-weld heat-treated base material, namely γ′ particles, MC-carbide, and eutectic γ-γ′ phases (Fig. 4) [23].

Fig. 8 shows the microstructure of the area around a crack, clearly indicating melting of the γ´ particles, which is a potential cause of the crack formation. In addition, a phase with a different chemical composition is observed at the end of the crack. Considering the potential role of this phase in the crack formation, EDS analysis was performed to determine the composition of the observed phase.

Fig. 9 presents the elemental distribution of different specimens. A zirconium-rich phase was observed along the crack grain boundaries, which could be an intermetallic Zr-based phase or a sulfur phase with the composition of $(Zr, Ti)_2$ (C, S) [25, 26]. Given the relatively low melting

point of these phases, either phase could affect the formation of the liquid phase. Previous research reported the role of these phases in the liquation and crack formation in Ni-based superalloys [12, 23]. However, the mechanism through which these phases are liquated is different from the partial melting of the γ′ particles. Zirconium-rich phases have a relatively low melting point. As a result, upon an increase in the temperature across the weld region, these phases are directly melted to form a liquid phase around the weld pool. This liquid phase may then penetrate the interphase boundaries and contribute to crack formation. Therefore, in addition to the γ′ particles, other phases, such as zirconium-rich phases, can affect the formation of liquid phases and cracks. The mechanism through which the zirconium-rich phase was developed along the grain boundaries is described in the following section.

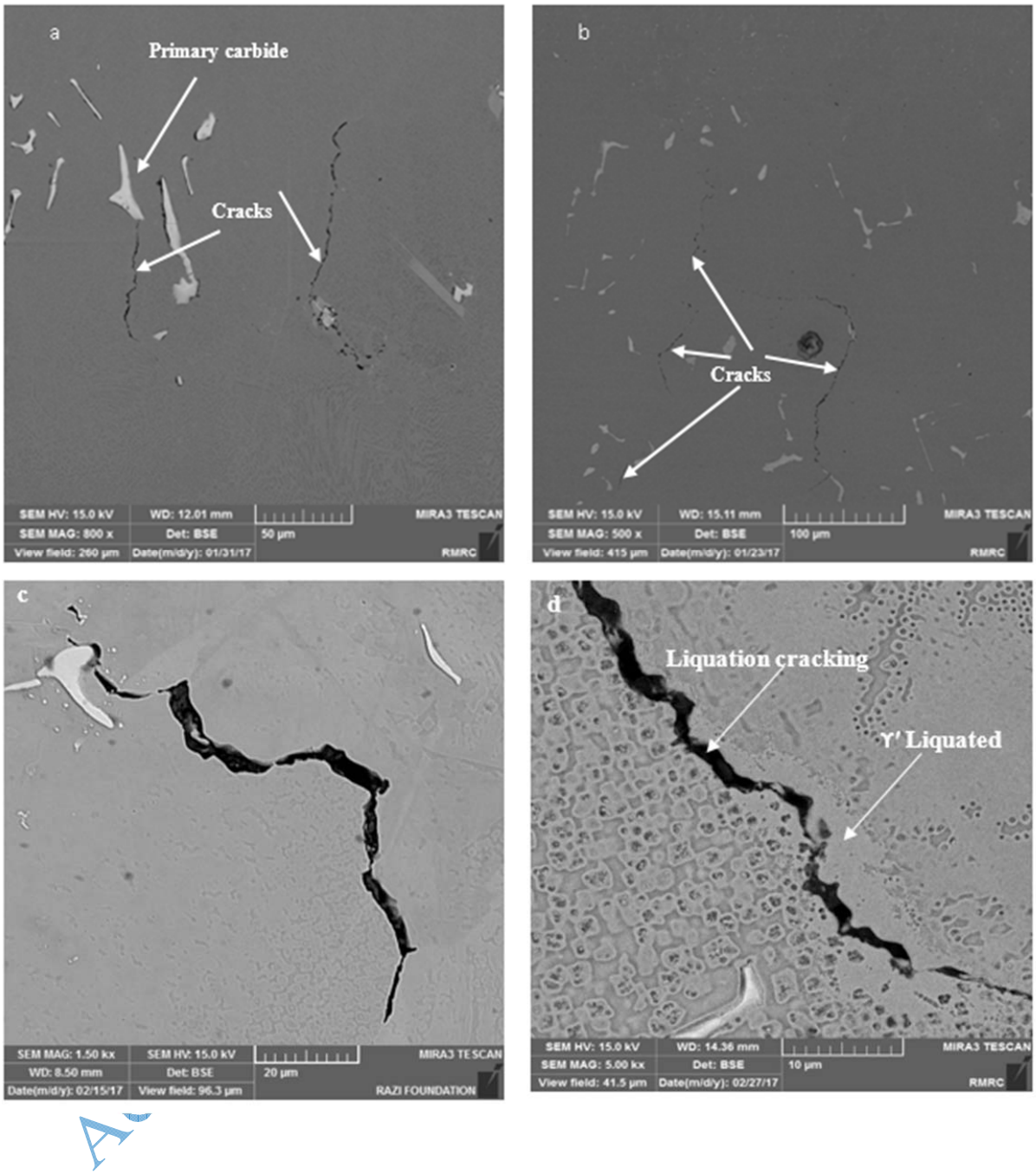

Figure 7. Liquation cracking in the samples welded with (a, c) Hastelloy X and (b, d) IN718 as filler metal. Intergranular cracking occurred around the particles of the secondary phases associated with the constitutional liquation mechanism.

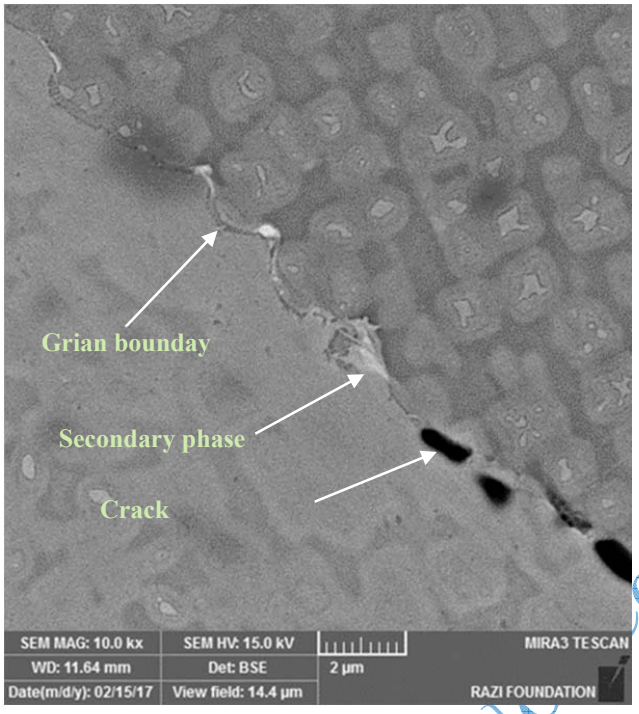

Figure 8. FESEM images of the sample welded with IN718 as filler metal. A different composition is evident at the end of the crack opening.

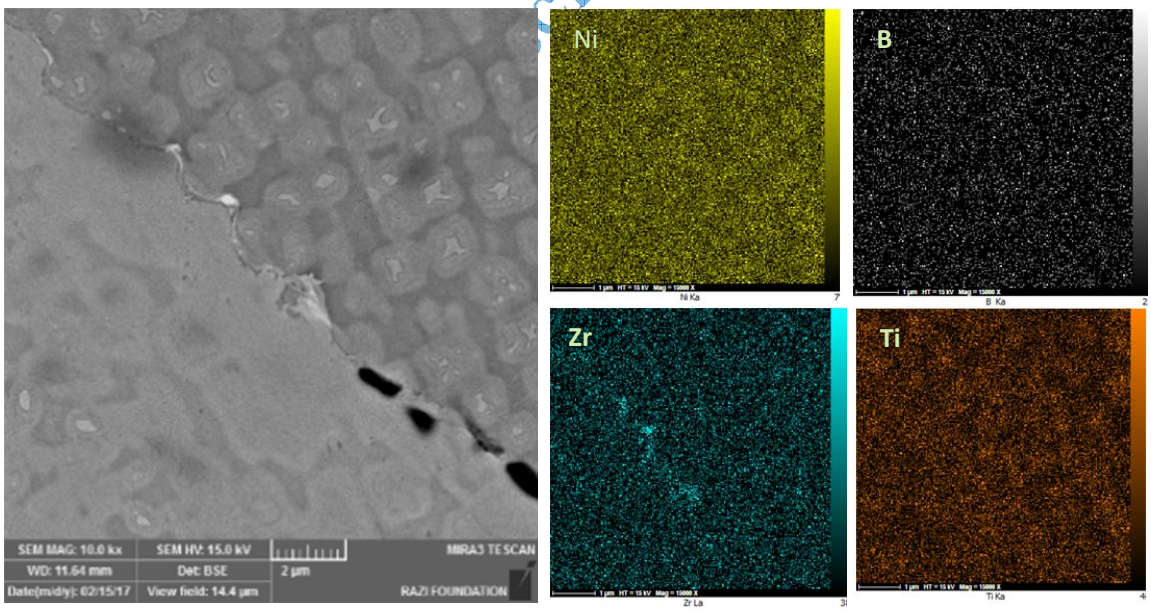

Figure 9. Energy-dispersive X-ray spectroscopy (EDS) map of the elements around the crack on the sample welded with IN718 as filler metal, indicating the presence of a zirconium-rich phase along the cracked grain boundaries.

The distribution of the solute in the solidification step can be explained by the Brody-Flemings and Scheil equations (Equations (1) and (2), respectively) [8]. For the Scheil Equation (2), we assume that the diffusion of solute particles into the solid solution is negligible.

$$C_S = KC_0 \left[1 - \frac{f_s}{1+\alpha K}\right]^{K-1} \quad (1)$$

$$C_S = KC_0 [1 - f_s]^{K-1} \quad (2)$$

where C_s is the solid composition at the solid/liquid interface, C_o is the nominal alloy composition, f_s is the solid fraction and K is the equilibrium partition ratio or the equilibrium segregation coefficient that describes the partitioning of an alloying element to liquid and solid phases during the solidification process. At any given temperature "T," K is calculated as follows [8, 20]:

$$K = \frac{C_S}{C_L} \quad (3)$$

Accordingly,

- if $K < 1$, the solid is expected to reject the solute into the liquid during the solidification process, and
- if $K > 1$, the solid is expected to absorb the solute from the liquid during the solidification process.

Table 3 provides calculated values of *K* for different elements at the start of the solidification process using the JMatPro Software. According to this table, Ni, Co, Cr, Fe, W, and Al correspond to *K* values greater than 1, while Mo, Si, Ti, Ta, Nb, and Zr end up producing *K* values less than 1. In addition, the Zr exhibits the lowest *K*. During the solidification process, the former elements are expected to be uniformly distributed in the core and interdendritic area given their *K* values, while the latter elements are expected to be rejected from the interdendritic area. Similar findings have been reported for other Ni-based superalloys [2]. The elemental distribution patterns obtained in this work are in close agreement with previous reports [2, 26-28]. Accordingly, the low-solubility elements, *e.g.,* Zr, were isolated in the final stages of solidification, leading to the formation of zirconide phases, *e.g.,* boron zirconium. In addition, low-solubility elements with very small *K* values, such as Zr, were segregated in the final stages of solidification, resulting in the formation of zirconide and boride phases, *e.g.*, M_3B_2 and Ni_7Zr_2

[2]. The microstructural observations further confirmed the presence of Zr phases in the cracks formed in the HAZ (Figs. 8 and 9).

3.2. Crack measurement and weld pool hardness

Fig. 10-a presents the crack measurements in terms of the total number of cracks and TCL on the pre-weld heat-treated samples with both filler metals. Although the welding conditions were identical for all of the specimens, different cracking configurations were observed in different samples, possibly due to different physical and mechanical properties of the weld pool. Specifically, the higher the hardness and strength of the weld pool, the less susceptible to crack formation during the welding process. In general, the filler metals increasing the welding stress are expected to increase the liquation cracking in the HAZ (Fig. 10-b).

Hastelloy X has a lower hardness than the IN718 given it is a solid solution. The hardness of the weld pools produced with Hastelloy and IN718 as a filler metal were 309 HV and 337 HV, respectively. Consistent with previous research [22-27], our studies of the cross-sections of the specimens welded by Hastelloy X showed no cracks in the HAZ (Fig. 10-a) because the ductility of the base metal led to lower stress of the welding process. A pre-weld heat treatment effectively reduces the HAZ cracking by reducing the hardness of the base metal and increasing its ductility.

Table 3. Calculated values of the equilibrium partition coefficients (K) using JMatPro for various elements in the weld fusion zone with different filler metals.

Filler metals	Ni	Al	Co	Cr	Fe	Mo	Nb	Si	Ta	Ti	W	Zr	Mn
IN718	1.03	1.09	1.11	1.04	1.14	0.62	0.24	0.56	0.22	0.52	0.99	0.032	
HASTELLOY X	1.06	1.1	1.05	1	1.12	0.62	0.23	0.53	0.22	0.51	0.88	0.04	

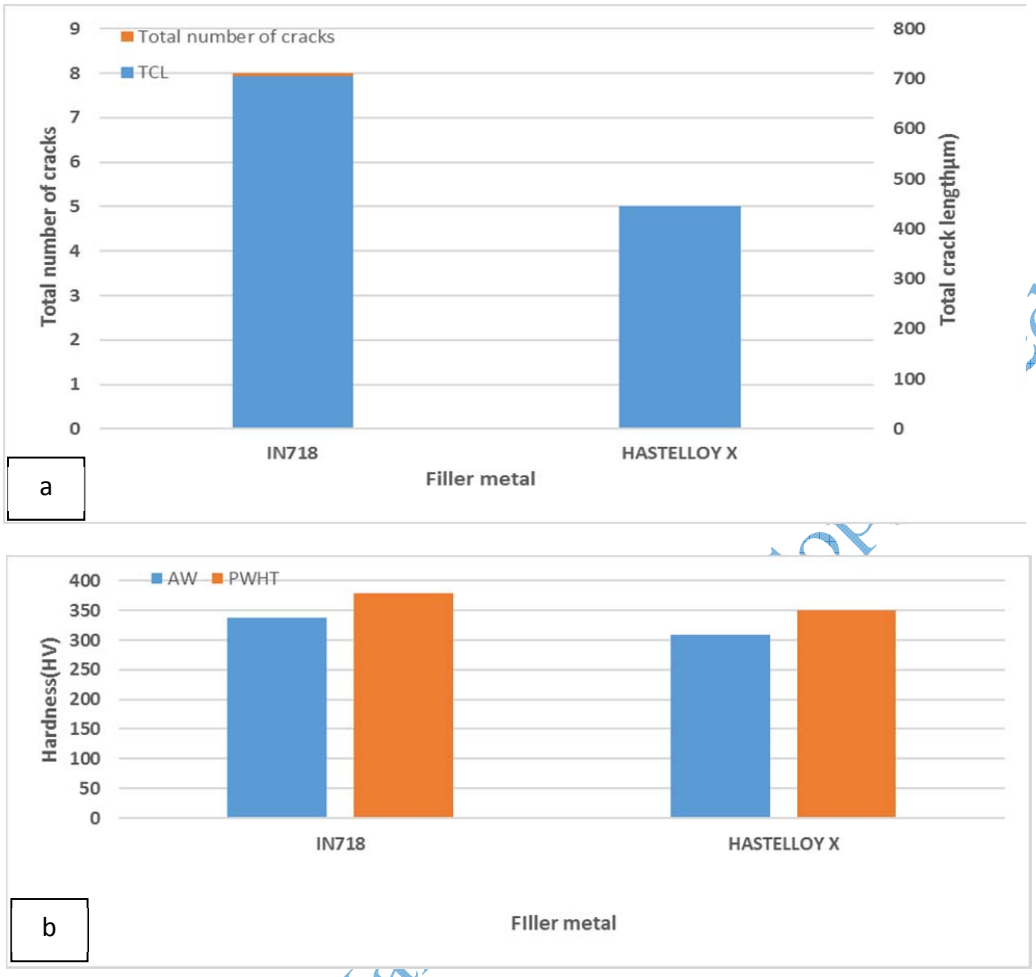

Figure 10. (a) Results of the crack investigation on the cross-section of the pre-weld heat-treated specimens welded with IN718 and Hastelloy X as filler metal, and (b) hardness of the weld pool for the as-weld (AW) and PWHT samples.

3.3. Chemical composition and microstructural examination of the weld pool

Given Hastelloy X is a solid solution, the hardness was expected to not change upon PWHT. However, the results indicate an increase in the hardness of the weld pool upon PWHT with both of the filler metals (Fig. 10-b), which could be related to changes in the chemical composition of the weld pool caused by dilution of the filler metal and base metal during the welding process. Table 4 presents the dilution (D) and chemical composition of the weld pool for various filler metals. During the welding process, Al and Ti (γ′ precursors) were fed from the base metal to the

weld pool, and then, during the PWHT process, the γ′ particles were formed, increasing the hardness of the weld pool.

To confirm the presence of the alloying elements in the weld pool, chemical investigations were performed using Energy Dispersive X-Ray (EDX) analysis. Table 5 shows the results of the EDX analysis on the weld pool, showing significantly higher concentrations of Al and Ti in the weld pool rather than the as-received filler metals. The results are consistent with the computed values of dilution and the microstructural studies (Table 3, Fig. 11).

The microstructure of the weld pools was examined by FESEM. Fig. 11 shows images of the γ′ particles (~ 0.2 μm) in the weld pools, indicating the formation of γ′ particles in the weld pools of both specimens after the PWHT. As previously mentioned, this is due to the intrusion of alloying elements, *e.g.,* Al and Ti as γ′ precursors, from the base metal to the weld pool and dilution with filler metal during the welding process (Table 5).

Table 4. Dilution levels (D) and chemical compositions of the weld pools (wt. %) per calculations by JMatPro.

Weld pool	D%	Cr	Ni	Co	Mo	W	Nb	Ti	Al	Fe	Ta	Al+Ti
IN718	65	22.28	48.86	12.7	1.05	1.43	2.5	2.72	1.48	5.86	0.91	4.2
HASTELLOY X	63	22.32	47.68	12.53	3.33	1.61	0.69	2.33	2.00	6.98	0.88	4.33

Table 5. Chemical composition of the weld pool per the EDX analysis (wt. %).

Weld pool	Cr	Ni	Co	Mo	W	Nb	Ti	Al	Fe	Other	Al + Ti
IN718	21.69	48.07	12.92	1.63	1.82	2.49	3.43	1.73	5.17	1.03 Ta	5.16
HASTELLOY X	22.36	45.18	12.34	4.82	1.12	1.05	2.73	1.56	6.42	2.41 Ta	4.29

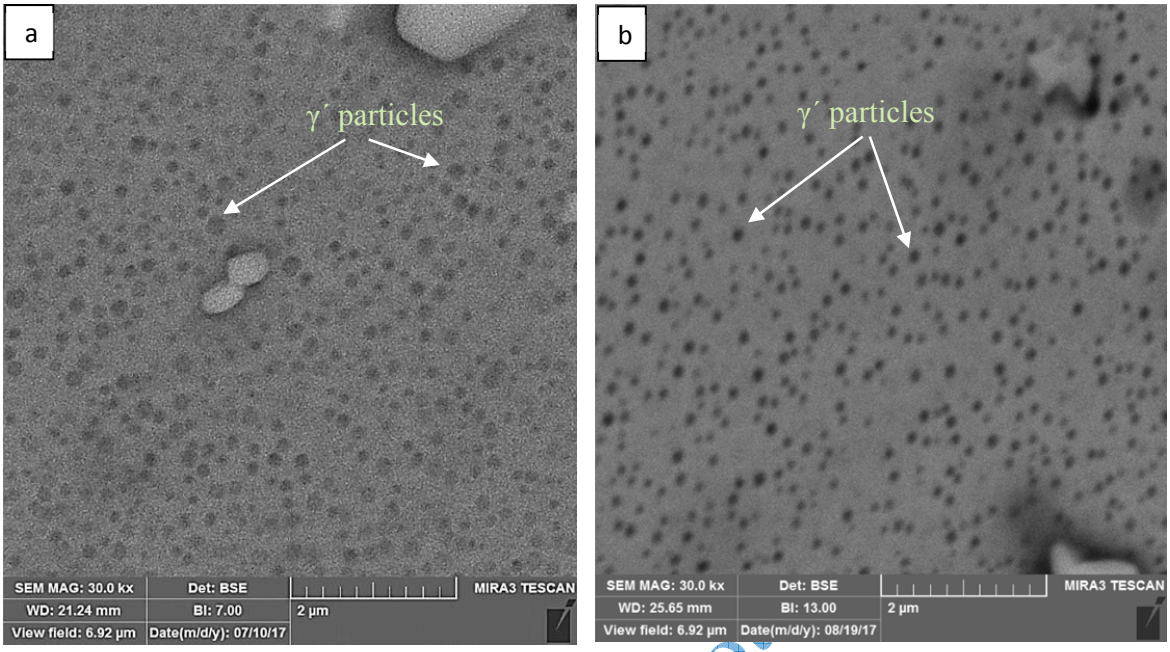

Figure 11. FESEM micrographs indicating the formation of γ′ particles in the weld pools of the samples welded with (a) IN718 and (b) Hastelloy X as a filler metal after the PWHT.

3.4. Physical properties of the weld pool and HAZ cracking

Variations of the γ and γ′ lattice parameters with temperature (from room temperature to 1100°C, simulated by JMatPro Software) in the weld pool are presented in Fig. 12 for both filler metals. Compared to the γ′ precipitate, the lattice parameter of the γ matrix increased more rapidly with temperature [30], as shown in Figs. 12-a and b. According to Fig. 12-a, when Hastelloy X and IN718 were used as filler metal, variations of the γ lattice parameters with temperature closely resembled those of the base metal (IN939). However, according to Fig. 12-b, when Hastelloy X was used as a filler metal, variations of the γ′ lattice parameters in the γ′ precipitation temperature range (<1000°C) closely resembled those of the base metal (IN939). As a result, with Hastelloy X as filler metal, the γ, and γ′ lattice parameters exhibited quite different behaviors than those of the base metal.

The lattice mismatch (δ) is an important factor in determining the morphology of the γ′ precipitate and is calculated by [29]:

$$\delta = \frac{2\left(a_{\gamma'} - a_{\gamma}\right)}{a_{\gamma'} + a_{\gamma}} \qquad (4)$$

where $a_{\gamma'}$ and a_{γ} are the lattice parameters of the γ′ and γ phases, respectively. Variations of the γ/γ′ mismatch with temperature in the weld pool are presented in Fig. 12-c. The γ/γ′ mismatch in the weld pool for Hastelloy X and IN718 filler metals are about 0.3 and 0.75 at room temperature, respectively. Accordingly, the γ′ particles in the weld pool for Hastelloy X and IN718 filler metals are expected to be cubic [29] based on the microstructural study. Fig. 12 shows a relatively constant γ/γ′ mismatch for both filler metals at temperatures up to about 600°C. At higher temperatures, a sharp decline was estimated because of the lower expansion coefficient of the γ′ phase compared to the γ phase [30]. With the mismatch of a lattice indicating the amount of strain energy stored at the interface between γ and γ′ phases [30], a filler metal producing a closer mismatch to that of the base metal is expected to generate less strain in the weld pool, making the weldment less susceptible to cracking. Since the variations of the γ and γ′ lattice parameters were closer to those of the base metal (IN939) when the Hastelloy X was used as filler metal, this alloy was expected to have the smallest γ/γ′ lattice mismatch (Fig. 12-c) and hence, strain in the HAZ. Alternatively, when used as filler metal, IN718 produced the largest γ/γ′ lattice mismatch (Fig. 12-c). These results are consistent with the metallographic studies and crack measurements. Other investigators have reported the effect of γ/γ′ mismatch on the liquation cracking [16].

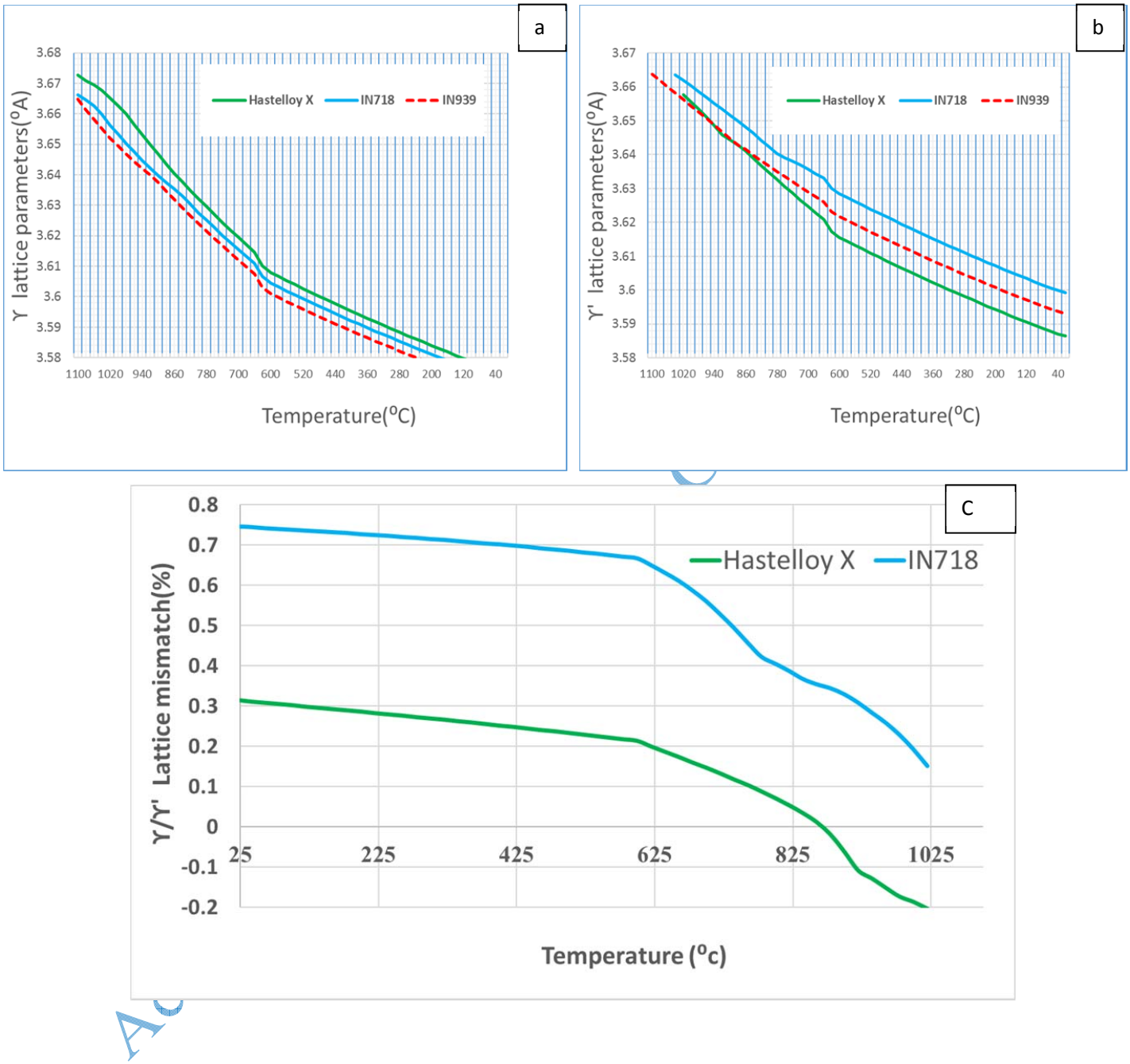

Figure 12. Variations of the lattice parameters with temperature (from room temperature to 1100°C) in the weld pool for IN718 and Hastelloy X filler metals: (a) γ, (b) γ′, and (c) γ/γ′ lattice mismatch.

4. Summary and conclusions

A summary of the present study is given below:

1. The pre-weld heat treatment results indicated complete dissolution of the secondary γ′ particles in the matrix and the growth of primary γ′ particles in the form of "ogdoadically diced cubes" with a side length of about 2 μm. Accordingly, the base metal hardness was reduced to 310 HV, which can help reduce crack formation during the welding process by increasing the ductility of the base metal and hence reducing the welding stresses.
2. The constitutional melting of secondary phases, *e.g.*, MC-carbide and γ′ particles, the eutectic γ- γ″ phase and the low melting phases, *e.g.*, zirconium-rich phase, led to liquation cracking in the HAZ of IN939 during TIG welding.
3. The γ′ particles of about 0.2 μm in size were observed in all weld pools. These phases increased the hardness of the weld pools after PWHT to about 350 and 380 HV for the Hastelloy X and IN718 filler metals, respectively.
4. Compared to Hastelloy X, the amount of liquation cracking in the HAZ is greater when IN718 is used as filler metal.

Acknowledgment

The authors would like to acknowledge the assistance from the Niroo Research Institute for providing the required research facilities.

Conflict of interest

The authors declare that they have no conflicts of interest.

References

1. T.Á. Tejedor, R. Singh, and P. Pilidis, *Modern Gas Turbine Systems,* Woodhead Publishing Series in Energy, New Delhi, 2013.
2. O. Ojo, N. Richards, and M. Chaturvedi, Microstructural study of weld fusion zone of TIG welded IN 738LC nickel-based superalloy, *Scr. mater.*, 51(2004), p. 683.
3. R. K. Sidhu, O. A. Ojo, N. L. Richards and M. C. Chaturvedi, Metallographic and OIM study of weld cracking in GTA weld build-up of polycrystalline, directionally solidified and single crystal Ni based superalloys, *Sci. Technol. Weld Joi.*, 14(2009), p. 125.
4. R. K. Sidhu, O. Ojo, and M. Chaturvedi, Microstructural response of directionally solidified René 80 superalloy to gas-tungsten arc welding, *Metall. Mater. Trans. A*, 40(2009), p. 150.
5. K.C. Chen , T.C. Chen, R.K. Shiue and L.W. Tsay, Liquation Cracking in the Heat-Affected Zone of IN738 Superalloy Weld, *Met.*, 8(2018), p. 387.
6. T. Gibbons, and R. Stickler, *IN939: Metallurgy, properties and performance, High Temperature Alloys for Gas Turbines 1982,* Springer, London, 1982.
7. C. Cutler and S. Shaw, The interrelationship of γ′ size, grain size and mechanical properties in IN-939, a cast nickel-base superalloy,*[in] the 5th International Conference, Strength of Metals and Alloys, Aachen*, 1979, p. 1357.
8. J.C. Lippold, S.D. Kiser, and J.N. DuPont, *Welding metallurgy and weldability of nickel-base alloys*. John Wiley & Sons, New Jersey, 2011.
9. O. Ojo, N. Richards, and M. Chaturvedi, Study of the fusion zone and heat-affected zone microstructures in tungsten inert gas-welded INCONEL 738LC superalloy, *Metall. Mater. Trans. A*, 37(2006), p. 421.
10. Q. Li, X. Lin, X. Wang , H. Yang, M. Song and W. Huang, Research on the grain boundary liquation mechanism in heat affected zones of laser forming repaired K465 nickel-based superalloy, *Met.*, 6(2016), p. 64.
11. O. Ojo, Y. Wang and M. Chaturvedi, Heat affected zone liquation cracking in electron beam welded third generation nickel base superalloys, *Mat. Sci. Eng. A*, 476(2008), p. 217.
12. M. Montazeri and F. Ghaini, The liquation cracking behavior of IN738LC superalloy during low power Nd: YAG pulsed laser welding, *Mater. Charact.*, 67(2012), p. 65.
13. M. Montazeri, F.M. Ghaini, and O. Ojo, Heat input and the liquation cracking of laser welded IN738LC superalloy, *Weld. J.*, 92(2013), p. 258.
14 O. Ojo, Intergranular liquation cracking in heat affected zone of a welded nickel based superalloy in as cast condition, *J. Mater. Sci. Technol.*, 23(2007), p. 1149.
15. O. Ojo and M. Chaturvedi, Liquation microfissuring in the weld heat-affected zone of an overaged precipitation-hardened nickel-base superalloy, *Metall. Mater. Trans. A*, 38(2007), p. 356.
16. M. A. González Albarrán, D. Martínez, E. Díaz, J.C. Diaz, I. Guzmán, E. Saucedo, A. Ma. Guzman, Effect of preweld heat treatment on the microstructure of heat-affected zone (HAZ) and weldability of Inconel 939 superalloy, *J. Mater. Eng. Perform.*, 23(2014), p. 1125.
17. M.A. González Albarrán, D. Martíneza, A. Péreza, H. Guajardob, A. Garzac, Microstructural response to heat affected zone cracking of prewelding heat-treated Inconel 939 superalloy, *Mater. Charact.*, 62(2011), p. 1116.
18. A.Thakur, *Microstructural responses of a nickel-base cast IN-738 superalloy to a variety of pre-weld heat-treatments* [Dissertation], Manitoba University, Winnipeg, 1997.
19. A. Thakur, N. Richards, and M. Chaturvedi, On Crack-Free Welding of Cast Inconel 738. *In. J. Joi. Mat.*, 15(2003), p. 21.
20. S. Kou, *Welding metallurgy,* John Wiley & Sons, New Jersey, 2003.
21. R. Ricks, A. Porter and R. Ecob, The growth of γ′ precipitates in nickel-base superalloys, *Acta Metall.*, 31(1983), p. 43.

22. M. Doi, T. Miyazaki, and T. Wakatsuki, The effect of elastic interaction energy on the morphology of γ′ precipitates in nickel-based alloys, *Mater. Sci. Eng.*, 67(1984), p. 247.
23. O. Ola, , O. Ojo, and M. Chaturvedi, On the development of a new pre-weld thermal treatment procedure for preventing heat-affected zone (HAZ) liquation cracking in nickel-base IN 738 superalloy, *Philos. Mag.*, 94(2014), p. 3295.
24. P. Petrzak, K. Kowalski, and M. Blicharski, Analysis of phase transformations in Inconel 625 alloy during annealing, *Acta Phys. Pol. A*, 4(2016), p. 1041.
25. H. Li and T. Chaki, Grain Boundary Melting and Hot Cracking in Weld Haz of A Two-Phase Ni 3 Al Alloy Containing Zr,*[in]*. MRS Online Proceedings Library Archive, **364(**1994).
26. S. A. David, J. M. Vitek, S. S. Babu, L. A. Boatner and R. W. Reed, Welding of nickel base superalloy single crystals, *Sci. Technol. Weld Joi.* , 2(1997), p. 79.
27. S. Babu, S. David, J. Vitek, M. Miller, Atom-probe field-ion microscopy investigation of CMSX-4 Ni-base superalloy laser beam welds, J. *de Phys. IV*, 6(1996), p. C5-253.
28. R. Nakkalil, N. Richards, and M. Chaturvedi, Fusion zone microstructure of electron beam welded incoloy 903, *Scr. Metall. Mater.*, 26(1992), p. 545.
29. B. Geddes, H. Leon, and X. Huang, *Superalloys: alloying and performance*, ASM International, Ohio, 2010.
30. M. Nathal, R. Mackay, and R. Garlick, Temperature dependence of γ-γ'lattice mismatch in nickel- base superalloys, *Mater. Sci. Eng.*, 75(1985), p. 195.